2000-01-5609

The Role of Constraints in the MDO of a Cantilever and Strut-Braced Wing Transonic Commercial Transport Aircraft

A. Ko, B. Grossman and W.H. Mason
Multidisciplinary Analysis and Design (MAD) Center for Advanced Vehicles
Department of Aerospace and Ocean Engineering, Virginia Polytechnic Institute and State University

R. T. Haftka
Department of Aerospace Engineering, Mechanics and Engineering Sciences, University of Florida

2000 World Aviation Conference
October 10-12, 2000
San Diego, CA

SAE The Engineering Society For Advancing Mobility Land Sea Air and Space® INTERNATIONAL

SAE International
400 Commonwealth Drive
Warrendale, PA 15096-0001 U.S.A.

AIAA
American Institute of Aeronautics and Astronautics
370 L'Enfant Promenade, S.W.
Washington, D.C. 20024

Published by the American Institute of Aeronautics and Astronautics (AIAA) at 1801 Alexander Bell Drive, Suite 500, Reston, VA 22091 U.S.A., and the Society of Automotive Engineers (SAE) at 400 Commonwealth Drive, Warrendale, PA 15096 U.S.A.

Produced in the U.S.A. Non-U.S. purchasers are responsible for payment of any taxes required by their governments.

ISSN #0148-7191

All AIAA papers are abstracted and indexed in International Aerospace Abstracts and Aerospace Database.

All SAE papers, standards and selected books are abstracted and indexed in the Global Mobility Database.

Copies of this paper may be purchased from:

AIAA's document delivery service
Aeroplus Dispatch
1722 Gilbreth Road
Burlingame, California 94010-1305
Phone: (800) 662-2376 or (415) 259-6011
Fax: (415) 259-6047

or from:

SAExpress Global Document Service
c/o SAE Customer Sales and Satisfaction
400 Commonwealth Drive
Warrendale, PA 15096
Phone: (724) 776-4970
Fax: (724) 776-0790

SAE routinely stocks printed papers for a period of three years following date of publication. Quantity reprint rates are available.

2000-01-5609

The Role of Constraints in the MDO of a Cantilever and Strut-Braced Wing Transonic Commercial Transport Aircraft

A. Ko,
B. Grossman, and W.H. Mason
Multidisciplinary Analysis and Design (MAD) Center for Advanced Vehicles
Department of Aerospace and Ocean Engineering
Virginia Polytechnic Institute and State University

R.T. Haftka
Department of Aerospace Engineering, Mechanics and Engineering Sciences
University of Florida

ABSTRACT

This study examines the role of different design constraints applied to the multidisciplinary design optimization of a strut-braced wing (SBW) transonic passenger aircraft. Four different configurations are examined: the reference cantilever wing aircraft, a fuselage mounted engine SBW, a wing mounted engine SBW, and a wingtip mounted engine SBW. The mission profile was for 325-passengers, Mach 0.85 and a 7500 nautical mile range with a 500 nautical mile reserve.

The sensitivity of the designs with respect to the individual design constraints was calculated using Lagrange multipliers. A design space visualization technique was also used to gain insight into the role of the different constraints in determining the design configuration. This design visualization technique uses a classic 'thumbprint' plot to represent the design space.

As expected, all the designs are very sensitive to the range constraint. The designs are also sensitive to the field performance constraints. The design visualization revealed that the second segment climb gradient constraint was a limiting factor in all the designs. It was also found that the wing mounted engines SBW and tip mounted engines SBW designs are more constrained than the cantilever wing optimum and fuselage mounted engines SBW designs.

INTRODUCTION

Transonic passenger transport aircraft designs over the past 50 years have utilized the same general configuration, the cantilever low wing concept. Keeping the general layout the same, advances in this concept have relied on advances in individual technologies, such as better engines, airfoil designs, high lift devices and control system alternatives. It is quite unlikely that major improvements in performance will occur if new design configurations are not considered in the transonic passenger transport aircraft industry. One such design configuration is the strut-braced wing design concept. Although this design configuration is common among small general aviation aircraft, it is rare in the large passenger transport arena.

The idea of using a truss-braced wing configuration for a transonic transport originated with Werner Phenninger [1] at Northrop in the early 1950s. The strut-braced wing (SBW) concept can be considered a subset of the truss-braced wing configuration. Other SBW aircraft investigations followed Phenninger's work, notably by Kulfan et al. [2] and Park [3] in 1978. Turriziani et al. [4] considered the advantages of the strut-braced wing concept on a subsonic business jet with an aspect ratio of 25. He found that the strut-braced wing concept achieved approximately 20% in fuel savings compared to a similar cantilevered subsonic business jet.

Recently, multidisciplinary design optimization (MDO) was employed to take advantage of the interaction between the various disciplines (such as aerodynamics and structures) in the design of a SBW passenger transport aircraft [5]. The Virginia Tech Multidisciplinary Analysis and Design Center, motivated by discussions with Dennis Bushnell, the Chief Scientist at NASA Langley, used MDO to design such an aircraft. As a result, it was found that the SBW concept provided significant savings in take-off gross weight compared to a similarly designed cantilever transport aircraft. Studies [5], [6] found that the SBW configuration allowed for a wing with higher aspect ratio and decreased wing thickness without any increase in wing weight relative to its cantilevered wing counterpart. Building on this work, a joint study by Lockheed Martin Aeronautical Systems (LMAS) and Virginia Tech showed that a fuselage mounted engines SBW configuration had a 9% savings in TOGW over the cantilever baseline. Details of this work can be found in references [7] and [8].

Innovative structural concepts are required to eliminate the possibility of strut buckling under the -1*g* and taxi bump cases. These structural considerations are described by references [9] to [11].

To better understand the MDO process in the design of the SBW aircraft, a study on the effects of the design constraints were performed. This paper illustrates the importance of different design constraints (such as field performance constraints) on the overall MDO process and the design evolution of the SBW aircraft. This approach helps connect MDO to traditional aircraft sizing.

DESIGN OPTIMIZATION

GENERAL ASPECTS

The design of the SBW aircraft uses an MDO approach to take advantage of the coupling between aerodynamics, structures and performance. The objective of the optimization is to minimize the take-off gross weight (TOGW) of the aircraft. This is the traditional objective of large transport designs and is a good general measure for a robust system [12]. Four different aircraft configurations are considered: the reference cantilever wing, fuselage mounted engines SBW, wing mounted engines SBW, and tip mounted engines SBW. The cantilever wing design is used as a baseline comparison for the SBW designs, and also as a validation case with which we can compare with existing aircraft. The mission profile of the designs was for 325-passengers, Mach 0.85 and a 7500 nautical mile range with a 500 nautical mile reserve. Figure 1 shows a summary diagram of the mission profile. The Virginia Tech SBW code uses the method of feasible directions implemented in the Design Optimization Tools (DOT) software developed by Vanderplatts R&D [13] to perform the optimization of the design.

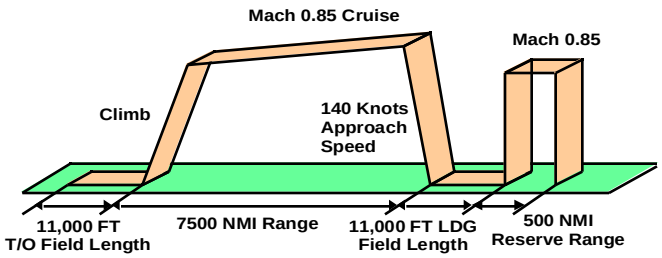

Figure 1: Aircraft Mission Profile

Depending on the configuration, a total of 15 to 22 design variables were employed. These include wing half-span, chords, thickness to chord ratios, strut position and geometry, engine location, thrust and cruise altitude. Each design variable is given upper and lower side constraints and then scaled to take a value between 0 and 1. Table 1 gives a list of all the design variables that are used for each of the different configurations.

Design Variables	Cantilever Optimum	Fuselage Mounted Engines SBW	Wing Mounted Engines SBW	Tip Mounted Engines SBW
Spanwise position of wing/strut intersection		✓	✓	✓
Wing semispan (ft)	✓	✓	✓	✓
Wing sweep (deg)	✓	✓	✓	✓
Strut sweep (deg)		✓	✓	✓
Strut chordwise offset (ft)		✓	✓	✓
Strut vertical aerodynamic offset (ft)		✓	✓	✓
Wing centerline chord (ft)		✓	✓	✓
Wing break chord (ft)	✓			
Wing tip chord (ft)	✓	✓	✓	✓
Strut chord (ft)		✓	✓	✓
Wing thickness to chord ratio at centerline	✓	✓	✓	✓
Wing thickness to chord ratio at breakpoint	✓	✓	✓	✓
Wing thickness to chord ratio at tip	✓	✓	✓	✓
Strut thickness to chord ratio		✓	✓	✓
Wing skin thickness at centerline (ft)	✓	✓	✓	✓
Strut tension force (lbs)		✓	✓	✓
Vertical tail scaling factor	✓	✓	✓	✓
Fuel weight (lbs)	✓	✓	✓	✓
Required thrust (lbs)	✓	✓	✓	✓
Spanwise position of engine		✓		
Average cruise altitude (ft)	✓	✓	✓	✓

Table 1: Design variables used in the different configurations.

AERODYNAMICS

The aerodynamics model consists of a combination of response surface equations developed from Computational Fluid Dynamics (CFD) analysis, traditional aerodynamics estimation methods, and theoretical models. The drag components that are addressed are parasite, induced, wave and interference drag. A detailed discussion of these drag models can be found in previous Virginia Tech SBW studies [6] and [14].

The parasitic drag model is based on applying form factors to an equivalent flat plate skin friction drag analysis. The amount of laminar flow on the wing and tails is estimated by interpolating results from the Reynolds number vs. sweep data obtained from the F-14 Variable Sweep Transition Flight Experiment (1984-1987) and the Boeing 757 Natural Laminar Flow Glove Flight Test (1985) [15]. For the fuselage, nacelles and pylon friction drag, an input Reynolds number is used to determine the transition location on those components.

To calculate induced drag, a discrete vortex method in the Trefftz plane [16] was used. This gives the optimum load distribution corresponding to the minimum induced drag for an arbitrary, non-coplanar wing/truss configuration.

For the wave drag calculation, the Korn equation, modified to include sweep using simple sweep theory is used [17], [18]. This model estimates the drag divergence Mach number as a function of airfoil technology factor, thickness to chord ratio, section lift coefficient, and sweep angle. The wave drag coefficient is calculated for a wing strip from the critical Mach number. Then, the total wave drag is found by integrating the wave drag of all the strips along the wing.

The interference drag of the wing, strut, and fuselage intersections are currently estimated using Hoerner equations based on subsonic wind tunnel tests [19]. In order to alleviate the problem associated with a sharp wing-strut angle, the strut employed here is given the shape of an arch and intersects the wing perpendicularly. Analyses for an arch radius varying from 1 ft to 4 ft were performed with CFD tools [20],[21]. Unstructured grids were obtained with the advancing-front methodology implemented in the code VGRIDns [22]. The Euler equations were solved using the CFD code USM3D [23], [24] at the cruise Mach number of 0.85. The drag penalty was obtained by subtracting the drag of the wing alone from the drag of the strut-braced wing design. The resulting number is a drag penalty associated with the presence of the strut. As the arch radius is increased, the drag penalty decreases almost exponentially. From these results, a curve fit is produced and used in the present analysis to account for the drag of the wing-strut junction.

STRUCTURES

Existing weight calculation models for the wing bending material weight (such as the NASA Langley developed FLOPS [25]) are inadequate to accurately predict the wing weight of the SBW aircraft due to its unconventional wing concept. Hence, a special wing bending weight model was created to take into account the influence of the strut on the structural wing design [9]. Also, a vertical strut offset (at the wing-strut junction) was modeled in an effort to reduce the wing/strut interference drag.

Previous studies on the strut-braced wing concept [3] revealed that to prevent strut buckling, the strut thickness had to be increased significantly. To address this strut-buckling problem, a telescoping sleeve mechanism was employed to allow the strut to be inactive in compressive loads. Only during positive *g* conditions does the strut activate.

To calculate the bending material weight, a piecewise linear beam model, representing the wing structure as an idealized double plate model, was used. Structural optimization is implemented to distribute the bending material based on three load cases, the 2.5*g* maneuver, -1.0*g* pushover and the -2.0*g* taxi bump. Since the strut is not active, high deflections in the wing are expected for the -2.0*g* taxi bump. To maximize the beneficial influence of the strut upon the wing structure, the strut force and spanwise position of the wing-strut intersection are optimized by the MDO code for the 2.5*g* maneuver case. Detailed description of the wing structures model can be found in reference [9].

WEIGHTS

To calculate the individual component weights of the aircraft, equations from NASA Langley's Flight Optimization System (FLOPS) [25] that were supplemented by LMAS, were used. These equations calculated the individual component weights such as the wing and fuselage weights. The wing bending material weight (from which the total wing weight is calculated) is obtained from the aforementioned wing-sizing module. Detailed discussion of the weight models can be found in [14].

PROPULSION

GE-90 class, high-bypass ratio turbofan engines are used in this study. Rubber engine sizing was used to scale the the engine to meet thrust requirements.

STABILITY AND CONTROL

FAR specifications require that an aircraft must be able to maintain straight flight at 1.2 times the stalling speed with one engine inoperative. It allows a maximum bank angle of 5° with some sideslip angle. The lateral force provided by the vertical tail provides most of the required yawing moment needed to maintain straight flight in an engine-out condition. However, for all the SBW configurations, circulation control is used on the vertical tail to augment the force provided by the vertical tail. The vertical tail lift coefficient due to circulation control is limited to an upper bound of 1.0. To calculate the stability derivatives, a modified DATCOM empirical method was used. Reference [26] provides a detailed explanation of the stability and control model.

PERFORMANCE

The range of the aircraft is calculated using the Breguet range equation. The cruise altitude is set as a design variable and hence is determined by the optimizer. To account for the fuel burned during the climb segment to initial cruise altitude, 95.6% of the Take-off Gross Weight (TOGW) is used as the weight of the aircraft in this calculation. For the *L/D* ratio, flight velocity and specific fuel consumption, values at an average cruising altitude and Mach number are used.

To calculate the initial cruise rate of climb, the altitude at initial cruise has to be determined. Since the average cruise altitude is set as a design variable, it can be used to calculate the initial cruise altitude using the following equation:

$$R/C_{Initial\ Cruise} = \left(\frac{T}{W} - \frac{1}{L/D}\right) M a \qquad (1)$$

where *T, W, L, D, a* and *M* are aircraft thrust, weight, lift, total drag, Mach number and speed of sound respectively. The Mach number and lift coefficient are assumed to be constant, which allows us to calculate the density and speed of sound at the initial altitude. The weight of the aircraft is 95.6% of the TOGW, and the *L/D* is assumed to be equal to the average cruise *L/D*.

The field performance analysis includes the calculation of the second segment climb gradient and the balanced field length. The second segment climb gradient requirement is defined as the ratio of the rate of climb to the forward velocity at full throttle while one engine is inoperative and with the gear retracted, over a 50 foot obstacle. When calculating the second segment climb gradient, the engine thrust is corrected for density and Mach number using a modified version of Mattingly's equation [27]. The balanced field length calculation is done based on an empirical estimation from Torenbeek [28].

The missed approach climb gradient is calculated using a method similar to that used for the second segment climb gradient. The difference in this calculation is that both engines are operating (instead of being in an engine out condition), and the weight of the aircraft is taken to be 73% of the TOGW.

For the approach velocity, it is taken to be 59.2% of the missed approach velocity, calculated while determining the missed approach climb gradient.

Landing distance is determined using methods suggested by Roskam and Lan [29]. It defines three legs in the landing distance calculation, the air distance, free roll distance and brake distance. The air distance is that distance from the 50 foot obstacle to the point of wheel touchdown, including the flare distance. The free roll distance is the distance between touchdown and the application of the brakes. The brake distance is the distance covered while the brakes are applied.

CONSTRAINTS

A total of 12 inequality constraints are used during the optimization process. These constraints reflect typical restrictions on passenger transport design. Table 2 lists the constraints. A brief description of each constraint is given below. Detailed descriptions regarding the individual constraints can be found in references [5], and [14].

Description	Constraint
Range	7500nmi + 500 nmi < Calculated Range
Initial Cruise Rate of Climb	Initial Cruise ROC > 500 ft/min
Cruise Max. Allowable Section C_L	Calculated Maximum Cruise C_L < 0.8
Fuel Capacity	Fuel Weight < Fuel Capacity
Engine-out	Required C_n < Available C_n
Wing deflection	Wing deflection < 20 ft.
Second Segment Climb Gradient	Calculated Gradient > 0.024
Balanced Field Length	Balanced Field Length < 11000 ft.
Approach Velocity	Approach Velocity < 140 knots
Missed Approach Climb Gradient	Calculated Gradient > 0.021
Landing Distance	Landing Distance < 11000 ft.
Slack Load Factor	0. < Strut Slack Load Factor < 0.8

Table 2: Optimization constraints

Range Constraint

The range constraint ensures that the aircraft meets the minimum range requirement in the mission profile. In this case, the minimum range is 7500 nmi with a 500 nmi reserve.

Initial Cruise Rate of Climb Constraint

This constraint requires that the available rate of climb at the initial cruise altitude be greater than 500 feet/second.

Maximum Allowable Cruise Section C_L Constraint

This constraint ensures that the required section maximum lift coefficient at cruise is less than a specified maximum section lift coefficient. In this case, we set the maximum section lift coefficient to have a value of 0.8.

Fuel Capacity Constraint

The fuel capacity constraint ensures that there is enough tank volume to meet the specified range. Fuel can be stored in nine different fuel tanks located in the fuselage (3 tanks), the wings (4 tanks) and the strut (2 tanks). The tanks in the wings are assumed to occupy 50% of the chord of the wing, in between the front and rear spars. These tanks are divided into spanwise strips to calculate their fuel weight distribution. In this study, no fuel is stored in the fuselage tanks. The optimized designs show that fuel tanks in the wings alone are sufficient to store the necessary fuel to meet range requirements.

Engine Out Constraint

The engine out constraint ensures that this FAR specification is met. Details of this analysis have been discussed in the previous section.

Wing Deflection Constraint

The wing deflection constraint ensures that the wing or the nacelles on the wing do not strike the ground during taxi. The maximum deflection is set to 20 feet for all the configurations. The actual deflection of the wing is obtained from the structures model using a piecewise linear beam model. The pylon and nacelles under the wings are considered when determining the lowest point on the wing.

Second Segment Climb Gradient Constraint

This constraint ensures that the FAR specifications, which require that the minimum second segment climb gradient for a twin engine passenger transport aircraft be equal to 0.024, be met.

Balanced Field Length Constraint

The balanced field length determines the takeoff distance of the aircraft. The constraint requires that the calculated balanced field length does not exceed the stipulated maximum field length. In this study, the maximum field length is set to 11,000 ft.

Approach Velocity Constraint

The approach velocity constraint limits the approach velocity of the aircraft to a maximum of 140 knots.

Missed Approach Climb Gradient Constraint

The missed approach climb gradient constraint restricts the missed approach climb gradient to be greater than the specified minimum value. The minimum missed approach climb gradient for a twin engine passenger transport aircraft specified in the FAR is 0.021.

Landing Distance Constraint

The landing distance constraint limits the landing distance of the aircraft to be less than the maximum balanced field length (11,000 ft).

Slack Load Factor Constraints

To prevent buckling, the strut is designed to take loads in tension only. In compression, the strut disengages under a certain load through a telescoping sleeve mechanism. This is necessary to prevent strut buckling. The slack load factor is defined as the load factor at which the strut initially engages. The slack load factor constraint ensures that the slack load factor remains in the region of 0 and 0.8. It was found that without this constraint, the optimizer chooses a slack load factor of approximately 1, which implies that the strut engages right at the cruise condition. This is undesirable since dynamic effects (such as gusts) would cause the strut to engage and disengage frequently in cruise. With a maximum slack load factor of 0.8, the strut will always be engaged most of the time in cruise.

RESULTS OF THE OPTIMIZATION

Figures 2 to 5 summarize the results obtained from the optimization. The wing mounted engines SBW aircraft gives the most savings in TOGW over a similarly designed cantilever aircraft at 14.3%. Fuel weight savings for this design is at 16%. Overall, the SBW aircraft provides significant savings in both TOGW and fuel weight over the cantilever aircraft.

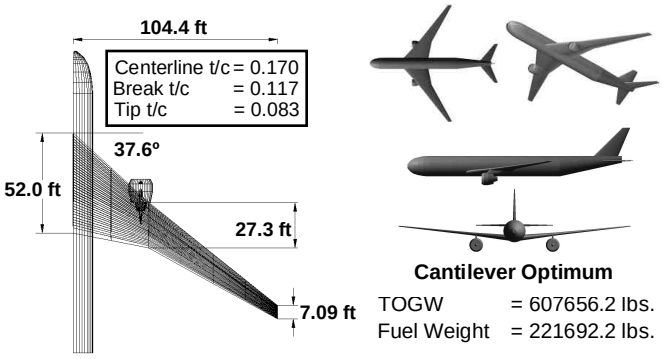

Figure 2: Optimized Cantilever Wing Aircraft Design.

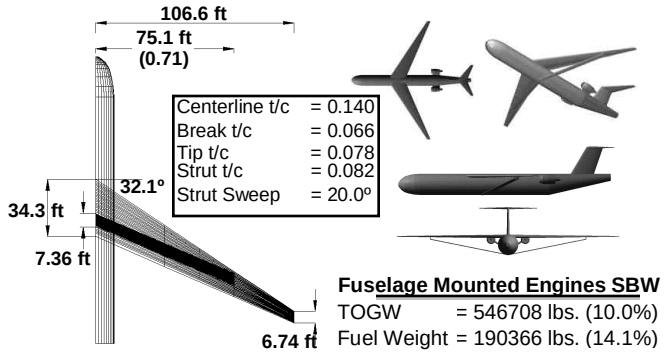

Figure 3: Optimized Fuselage Mounted Engines SBW Design. Percentages in parenthesis are comparisons with the optimized Cantilever Wing Aircraft.

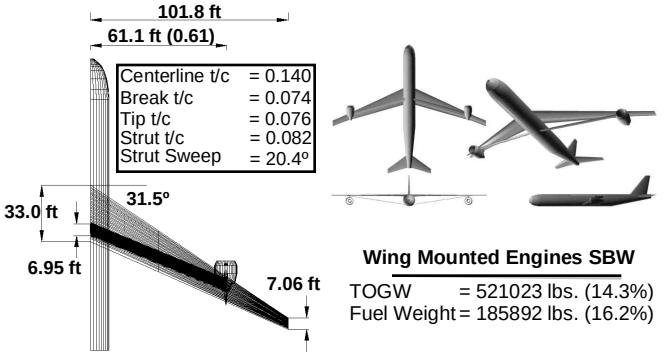

Figure 4: Optimized Wing Mounted Engines SBW Design. Percentages in parenthesis are comparisons with the optimized Cantilever Wing Aircraft.

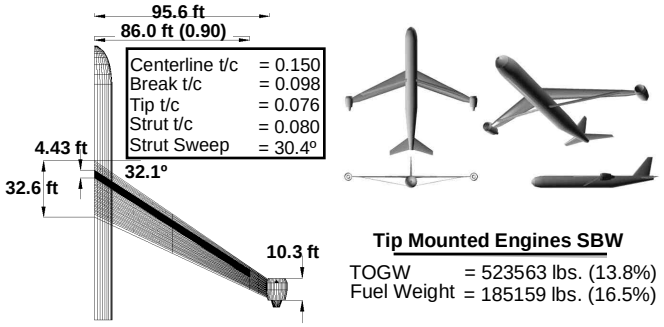

Figure 5: Optimized Tip Mounted Engines SBW Design. Percentages in parenthesis are comparisons with cantilever aircraft

Although these results look promising for the SBW concept, further study is needed to better understand the individual designs. To achieve this, a study of the effects of the constraints on the different optimized designs was done.

EFFECTS OF DESIGN CONSTRAINTS

METHODOLOGY

The sensitivities of the constraints were obtained by calculating the associated Lagrange multipliers. Techniques used to compute optimal sensitivity information are summarized in reference [30]. Although the optimizer uses the method of feasible directions (which does not calculate the Lagrange multipliers), the output obtained can be used to calculate the multipliers.

In general, the optimization problem can be mathematically represented in terms of the objective function (F), design variables (x_i), and the constraints (g_j) as

minimize F, where $F = F(x_1, x_2, \ldots x_n)$ for $I = 1, n$

subject to $g_{j\text{-limit}} \le g_j(x_1, x_2, \ldots x_n)$ for $j = 1, m$

This optimization problem leads to the optimality condition :

$$F(X) + \sum_{i=1}^{m} \lambda_j \quad g_j(X) = 0 \qquad (2)$$

Where λ_j are the Lagrange multipliers. It can be shown that the derivative of the objective function at the optimum point, F(X*) with respect to the constraint limit, $g_{j\text{-limit}}$ is equal to the Lagrange multiplier.

$$\frac{\partial F(X^*)}{\partial g_{j\text{-limit}}} = -\lambda_j \qquad (3)$$

To solve for the Lagrange multipliers, we can write the optimality equation in the form:

$$\{F(X^*)\} + [\ g(X^*)]\{\lambda\} = 0 \qquad (4)$$

Given **F(X*)** and **g(X*)**, we can solve for $\{\lambda\}$. To further simplify the problem, we know that if a constraint is inactive, its respective Lagrange multiplier will be zero. Hence, this reduces the number of unknowns to the number of active constraints. In light of this, when the number of equations exceed the number of unknowns, a least-square solution is obtained.

To compare the importance of various constraints, the logarithmic derivative was calculated. This is defined as

$$\frac{du}{dx} = \frac{d(\log u)}{d(\log x)} = \frac{du/u}{dx/x} \qquad (5)$$

The logarithmic derivative gives the percent change of the TOGW due to a percent change in the constraint. Therefore, we can use this derivative to compare the sensitivities of the designs with respect to the constraints, and identify the key constraints.

Since the constraints are normalized by the optimizer, the logarithmic derivative can be obtained by scaling the Lagrange multipliers by the TOGW of the designs. Also, to qualitatively represent the sensitivity of the derivatives, the Lagrange multipliers are unscaled by dividing each variable with its corresponding constraint limit.

RESULTS

Figure 6 shows the logarithmic sensitivity of all the constraints considered. The results show that the range constraint is the most important constraint, with a logarithmic sensitivity approximately six times larger than the next highest derivative. This is an expected result as the fuel weight is mainly determined by the range constraint. Also, since the range is a design requirement, we would expect this constraint to have a large impact on the designs.

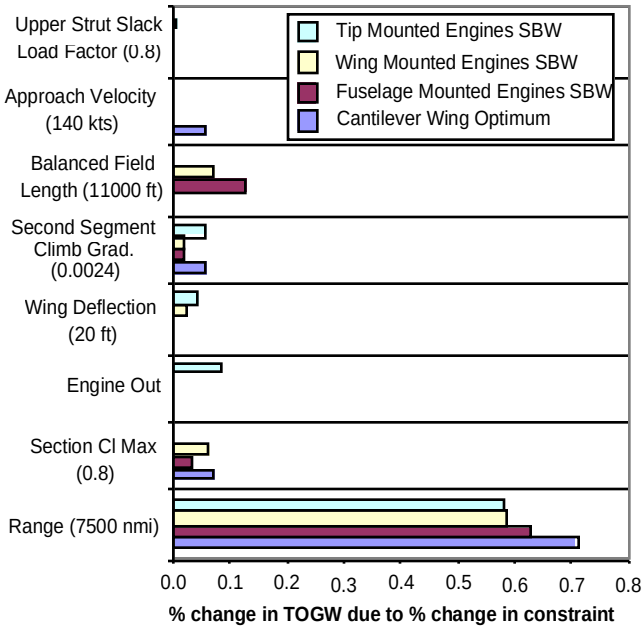

Figure 6: Logarithmic sensitivity of the design configuration with respect to the constraints

We can see that the balanced field length and second segment climb gradient constraint are also important. However, we find that where there is a comparison, the SBW designs are generally less sensitive to the constraints compared to the cantilever wing design. Only in the case of the balanced field length constraint is this not true. This is an important result as it implies that if the constraints are tightened, the SBW designs will incur a smaller penalty compared to the cantilever wing design. It would therefore allow designers more flexibility in the design of the SBW aircraft.

Table 3 gives a ranking of the different constraints for the designs. As mentioned earlier, the range constraint ranks the highest in all the constraints. Another trend that we see is that the slack load factor constraint is the least important constraint in the list for all three SBW designs (the slack load factor constraint does not apply to the cantilever design). Otherwise, there is no noticeable trend between the designs for the other constraints. This indicates that each design is distinct, and each design needs to be examined individually.

	Rankings			
	Cantilever Wing Optimum	**Fuselage Mounted Engines SBW**	**Wing Mounted Engines SBW**	**Tip Mounted Engines SBW**
1	Range	Range	Range	Range
2	Section Cl Max	Balanced Field Length	Balanced Field Length	Engine Out
3	Approach Velocity	Section Cl Max	Section Cl Max	Second Segment Climb Gradient
4	Second Segment Climb	Second Segment Climb Gradient	Wing Deflection	Wing Deflection
5	Balanced Field Length	Upper Strut Slack Load Factor	Second Segment Climb Gradient	Upper Strut Slack Load Factor
6			Upper Strut Slack Load Factor	Section Cl Max

Table 3: Table of rankings of the constraints for different aircraft configurations.

Table 4 shows the unscaled sensitivities of the designs with respect to the constraints. These values should only be compared between different designs for each constraint. This table gives the change in TOGW in pounds for a unit change in the constraint. For example, for the cantilever wing optimum, an increase in a nautical mile of range would result in a 57.7 lbs increase in TOGW. Another way of interpreting this is that a 10% decrease in range would result in a predicted reduction of TOGW by 43305lbs (750nmi×57.75lbs/nmi). On the other hand, increasing the cruise section $C_{l\,max}$ to 0.9 will reduce the weight by only 5724lbs. Table 3 provides us with an estimate with which we can use to predict the change in TOGW if the constraint limits are changed. The second segment climb gradient is shown twice, the first in units of lbs per radians, while the second listing has the units of lbs per degree. This is done to give the reader a better feel for the magnitude of the sensitivity.

Constraint	**Unscaled Sensitivities (lbs/*)**			
	Cantilever Wing Optimum	Fuselage Mounted Engines SBW	Wing Mounted Engines SBW	Tip Mounted Engines SBW
Range (7500 nmi)	57.74	46.12	40.53	41.22
Section Cl Max (0.8)	-57240	-23310	-41370	0
Engine Out	0.00	0.00	0.00	469400.00
Wing Deflection (20 ft)	0.0	0.0	-630.5	-1198.0
Second Segment Climb Grad. (0.0024)	1519000	452200	457800	1336000
Second Segment Climb Grad. (lbs/deg)	26520	7897	7994	23330
Balanced Field Length (11000 ft)	-0.16	-6.34	-3.51	0.00
Approach Velocity (140 kts)	-264.7	0.0	0.0	0.0
Upper Strut Slack Load Factor (0.8)	0.0	-556.6	-738.1	-5411.6

Table 4: Table of unscaled sensitivities of designs with respect to the constraints. Values in parenthesis indicate the constraint limit used in unscaling the sensitivities. The second listing of the second segment climb gradient is in units lbs/deg.

From Table 4, we find again that the SBW designs are generally less sensitive to the constraints compared to the cantilever wing aircraft.

Attention should also be given to the engine out constraint and approach velocity constraint. For the engine out constraint, only the tip mounted engines SBW design is active. This is expected due to the large yawing moments created due to the large separation of engine and centerline during an engine out condition. This result suggests that only the tip mounted engines SBW design would likely need the benefits of circulation control on the vertical tail (although in this study, circulation control on the vertical tail is included for all the designs). For the approach velocity constraint, only the cantilever wing design is active. It indicates that the SBW designs have a lower approach velocities than that of the cantilever aircraft.

To verify the sensitivities obtained, a comparison between the sensitivity estimate and the actual change in optimal solution was done for each of the constraints. The sensitivities generally match the optimal solution within a band of ± 10% (for the range constraint, the sensitivity is within ± 5% of the optimal solution). A detailed description of this comparison can be found in reference [31].

DESIGN SPACE VISUALIZATION

Although the constraint sensitivities allow us to gauge the impact of the constraints to the designs, it does not identify crucial constraints that limit the designs. To do this, a graphical interpretation of the design space is needed. A common tool used by aircraft designers to understand and visualize the design space is by making plots called 'carpet plots' or 'thumbprint plots'. In most preliminary designs efforts, these plots are used to select the best combination of thrust-to-weight ratio (*T/W*) and wing loading (*W/S*) that will give the lowest TOGW.

A 'thumbprint plot' is a contour plot of the TOGW at constant values of *T/W* and *W/S*. This is done once the aircraft configuration has been determined. While changing values of *W/S* and *T/W*, the aircraft is scaled to the meet the required mission range. In other words, while keeping the aircraft planform fixed, the aircraft wing is scaled in size to meet the range requirements. Constraint lines are also cross-plotted, showing feasible and infeasible regions. This allows the designer to analyze the aircraft's performance vs. the requirements.

In this study, thumbprint plots will be made to analyze the different configurations. Although the optimizer already provides us with the optimum configuration (and hence the best combination of *T/W* and *W/S* for the lowest TOGW), the plots will enable us to further understand the designs and identify critical constraints that limit the designs. It will also indicate how constrained each design is. While the sensitivity calculation discussed previously provide information on how sensitive the design is to each constraint, it does not indicate which constraint limits the design. In other words, although a design could be sensitive to a certain constraint, the design may not lie right against a constraint limit line. It is possible that this optimum design is within the 'active' band of the constraint (but not on its edge) since a certain tolerance level is used in determining if a constraint is active or not. Areas where the design is infeasible (i.e. the design violates one or more constraints) are darkened. It should be noted again that every point in the plot satisfies the range constraint. Therefore, a range constraint is not present in any of the plots.

Figure 7 shows the thumbprint plot corresponding to the cantilever wing optimum design. From the legend, we can see that the lowest TOGW design corresponds to a small *T/W* value. Hence, the area on the lower right of the plot represents the feasible region for the design. The plot shows that the optimum design provided by the optimizer is within the vicinity of the lowest TOGW feasible design. The plot also shows how the balanced field length, maximum cruise section C_L and second segment climb gradient constraint lines intersect at the lowest TOGW feasible design. This indicates that the design is well balanced, with the right combination of design variable values that exploits the constraints fully. It should be noted that the aircraft planform is fixed throughout this plot, and hence changing any of the design variables would change the constraint lines and the shape of the contours. We can also infer from this plot that the balanced field length, maximum cruise section C_L and second segment climb gradient constraint limits the design of the cantilever wing optimum aircraft. The approach velocity constraint, although indicated as an active constraint by the optimizer, does not limit this design.

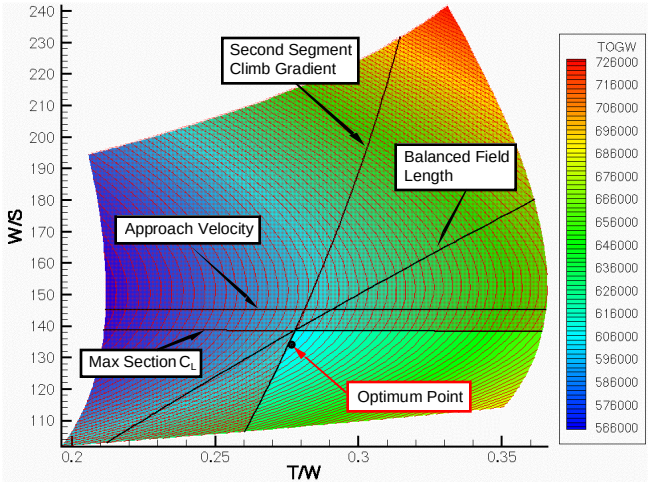

Figure 7: Thumbprint plot of the cantilever wing optimum design.

Figure 8 is the thumbprint plot for the fuselage mounted engines SBW design. The plot is very similar to that for the cantilever wing optimum, except that the minimum TOGW feasible design has a lower *T/W* value. Like the cantilever wing optimum, the balanced field length, maximum cruise section C_L and second segment climb gradient constraints limit the design, and their lines intersect each other at one point.

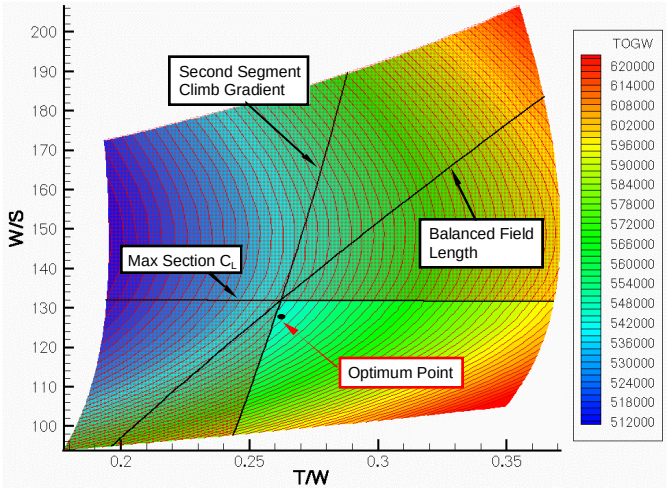

Figure 8: Thumbprint plot of the fuselage mounted engines SBW optimum design.

The thumbprint plot for the wing mounted engines SBW in Figure 9 is slightly different from the previous plots shown. First, the balanced field length constraint line does not intersect the maximum cruise section C_L and second segment climb gradient constraint lines at the same point, but is close to this point. Because of this, the minimum TOGW feasible design is

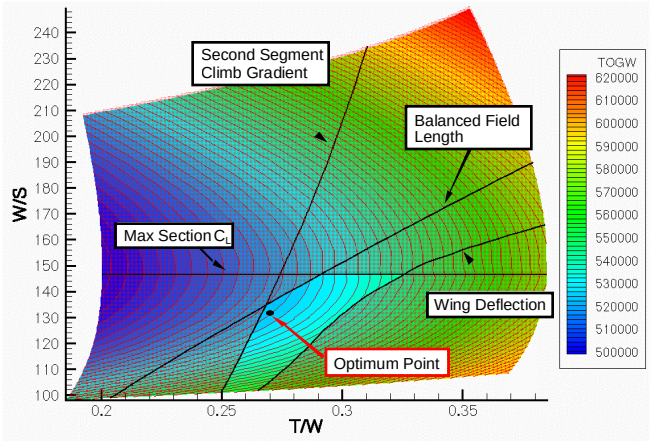

Figure 9: Thumbprint plot of the wing mounted engines SBW optimum design.

limited by the second segment climb gradient and balanced field length. If the balanced field length constraint is relaxed (i.e. moving the line higher and to the left), the minimum TOGW design will be limited by the maximum cruise section C_L constraint. It can be seen that the wing deflection constraint bounds the left side of the design space. We can expect this to happen since increasing the engine thrust (and hence increasing the value of *T/W*) would increase the weight of the engines on the wings. This would result in a larger wing deflection. In the case of *W/S*, increasing the wing area (and hence reducing the value of *W/S*), would size the wing with a larger span, and result in larger wing deflections. Although the wing deflection constraint does not limit the wing mounted engines SBW design, it causes the feasible design space to form a 'channel'. This smaller feasible design space is indicative of a more difficult optimization.

Figure 10 shows the thumbprint plot for the tip mounted engines SBW. In this plot, we find that there is only a small area where the design is feasible. This feasible space is bounded by the second segment climb gradient, engine out and wing deflection constraints. The small feasible design space for the tip mounted engines SBW explains why the tip mounted engines SBW configuration is the most difficult to optimize. The small feasible design space also indicates that there is little flexibility in the design from the optimum point without violating any of the constraints. Although the second segment climb gradient constraint limits this design, the engine out condition constraint bounds the feasible design space, and should also be considered an important constraint to consider for this configuration. The fact that the engine out condition constraint is only important for the tip mounted engines SBW case is expected, since we would expect large yawing moments during an engine out condition with the engines on the wing tips. As mentioned before, the vertical tails use circulation control to augment the yawing moment. One can expect the feasible design space to be smaller, or that the design would not have a feasible solution if

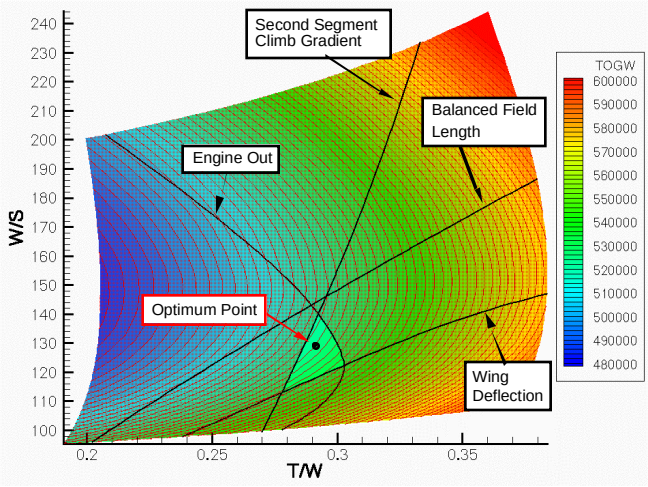

Figure 10: Thumbprint plot of the tip mounted engines SBW optimum design.

circulation control is not used for this SBW configuration.

From the thumbprint plots, we find one consistent trend in all the design configurations. This trend is that the second segment climb gradient constraint is a strong limiting factor in all of the designs. Since this constraint is a FAR requirement, the possibility of relaxing this constraint does not exist. In order to overcome or obtain more savings in TOGW, design factors that address the second segment climb gradient constraint should be considered. These factors include providing more engine thrust without incurring significant weight penalties and increasing the maximum lift to drag ratio at take-off.

CONCLUSIONS

A study of the effects of constraints in the multidisciplinary design optimization of a strut-braced wing transonic transport aircraft was done. The study was also done for a reference cantilever wing baseline aircraft. The study helped to understand the design process and its interdependencies between different aircraft design disciplines.

The study revealed that the designs are most sensitive to the range and field performance constraints. However, the use of a strut helps to reduce the penalties incurred by these constraints. In other words, the SBW design is less sensitive to most constraints than the cantilever wing design.

The design space visualzation technique that uses the concept of thumbprint plots provides insight into the driving factors of the aircraft design. It was found that in all the configurations, the second segment climb gradient constraint was the limiting factor. Also, it was found that the tip mounted engines SBW design was the most constrained from the four different configurations. The design space for the cantilever wing and fuselage mounted engines SBW designs are similar.

ACKNOWLEDGMENTS

This project was funded by NASA Langley Research Grant NAG-1-2217. b

CONTACT

Andy Ko
Multidisciplinary Analysis and Design (MAD) Center for Advanced Vehicles
Department of Aerospace and Ocean Engineering
Virginia Polytechnic Institute and State University
Blacksburg, VA 24061-0203, USA
Phone: (540) 231-6611
Fax: (540) 231-9632
Email: yko@aoe.vt.edu
http://www.aoe.vt.edu

REFERENCES

[1] Pfenniger, W., "Design Considerations of Large Subsonic Long Range Transport Airplanes with Low Drag Boundary Layer Suction," Northrop Aircraft, Inc.,

Report NAI-58-529 (BLC-111), 1958. (Available from DTIC as AD 821 759)

[2] Kulfan, R.M., and Vachal, J.D., "Wing Planform Geometry Effects on Large Subsonic Military Transport Airplanes," Boeing Commercial Airplane Company, AFFDL-TR-78-16, February 1978.

[3] Park, P.H., "The Effect on Block Fuel Consumption in a Strutted vs. Cantilever Wing for a Short Haul Transport Including Strut Aerolastic Considerations," AIAA Paper 78-1454, 1978.

[4] Turriziani, R.V., Lovell, W.A., Martin, G.L., Price, J.E., Swanson, E.E., And Washburn, G.F., "Preliminary Desing Characteristics of a Subsonic Business Jet Concept Employing an Aspect Ratio 25 Strut-Braced Wing," NASA CR-159361, October 1980.

[5] Grasmeyer, J.M., Naghshineh-Pour, A.H. Tetrault, P.A., Grossman, B.,Haftka, R.T., Kapania R.K., Mason, W.H., Schetz, J.A., "Multidisciplinary Design Optimization of a Strut-Braced Wing Aircraft with Tip-Mounted Engines," MAD Center Report 98-01-01, Virignia Tech, January 1998.

[6] Grasmeyer, J.M., "Multidisciplinary Design Optimization of a Strut-Braced Wing Aircraft", MS Thesis, Virginia Polytechnic Institute & State University, April 1998A.

[7] Martin, K.C., and Kopec, B.A., "A Structural and Aerodynamic Investigation of a Strut-Braced Wing Transport Aircraft Concept", Lockheed-Martin Aeronautical Systems, Marietta, GA, LG98ER0431, November 1998.

[8] Gundlach, J.F., Tetrault, P.A., Gern, F.H., Nagshineh-Pour, A., Ko, A., Schetz, J.A., Mason, W.H., Kapania, R.K., and Grossman, B., "Multidisciplinary Design Optimization of a Strut-Braced Wing Transonic Transport," AIAA Paper 2000-0420, *38th AIAA Aerospace Sciences Meeting and Exhibit*, Reno, NV, January 10-13, 2000.

[9] Naghshineh-Pour, A., "Structural Optimization and Design of a Strut-Braced Wing Aircraft," MS Thesis, Virginia Tech, November 1998.

[10] Gern, F.H., Gundlach, J.F., Ko, A., Naghshineh-Pour, A., Sulaeman, E., Tetrault P.A., Grossman, B.,Haftka, R.T., Kapania R.K., Mason, W.H., and Schetz, J.A., "Multidisciplinary Design Optimization of a Transonic Commercial Transport with a Strut-Braced Wing," SAE 1999-01-5621,*1999 World Aviation Congress*, San Francisco, CA, Oct. 19-21, 1999.

[11] Gern, F.H., Sulaeman, E., Naghshineh-Pour, A., Kapania, R.K., and Haftka, R.T., "Flexible Wing Model for Structural Wing Sizing and Multidisciplinary Design Optimization of a Strut-Braced Wing," AIAA Paper 2000-1427, *41st AIAA/ASME/ASCE/AHS/ASC Structures, Structural Dynamics, and Materials Conference and Exhibit*, Atlanta, GA, April 3-6,2000.

[12] Jensen, S.C., Rettie, I.H., and Barber, E.A., "Role of Figures of Merit in Design Optimization and Technology Assessment," *Journal of Aircraft*, Vol. 18, No. 2, February 1981, pp. 76-81.

[13] Vanderplaats Research and Development, Inc.,*DOT User's Manual*, Version 4.20, Colorado Springs, CO, 1995.

[14] Gundlach, J.F., Naghshineh-Pour, A.H., Gern, F., Tetrault, P.A., Ko, A., Schetz, J.A., Mason, W.H., Kapania R.K., Grossman, B.,Haftka, R.T., "Multidisciplinary Design Optimization and Industry Review of a 2010 Strut-Braced Wing Transonic Transport", MAD Center Report 99-06-03, 1999.

[15] Braslow, A.L., Maddalon, D.V., Bartlett, D.W., Wagner, R.D., and Collier, F.S., "Applied Aspects of Laminar-Flow Technology," *Viscous Drag Reduction in Boundary Layers*, AIAA, Washington D.C., 1990. pp. 47-78.

[16] Grasmeyer, J.M., "A Discrete Vortex Method for Calculating the Minimum Induced Drag and Optimum Load Distribution for Aircraft Configurations with Noncoplanar Surfaces," VPI-AOE-242, Department of Aerospace and Ocean Engineering, Virginia Polytechnic Institute and State University, Blacksburg, Virginia, 24061, January 1998.

[17] Mason, W.H., "Analytic Models for Technology Integration in Aircraft Design," AIAA-90-3262, September 1990.

[18] Malone, B. and Mason, W.H., "Multidisciplinary Optimization in Aircraft Design Using Analytic Technology Models," *Journal of Aircraft*, Vol. 32, No. 2, March-April 1995, pp. 431-438.

[19] Hoerner, S. F., *Fluid-Dynamic Drag: Practical Information on Aerodynamic Drag and Hydrodynamic Resistance*, pp. 8-1-8-20, published by S.F. Hoerner, Bakersfield, CA, 1965.

[20] Tetrault, P.A., "Numerical Prediction of the Interference Drag of a Streamlined Strut Intersecting a Surface in Transonic Flow," Ph.D. dissertation, Virginia Polytechnic Institute & State University, 2000. (Available at http://etd.vt.edu)

[21] Tetrault, P.A., Schetz, J.A., and Grossman, B., "Numerical Prediction of the Interference Drag of a Streamlined Strut Intersecting a Surface in Transonic Flow," AIAA Paper 2000-0509, *38th AIAA Aerospace Sciences Meeting and Exhibit*, Reno, NV, January 10-13, 2000.

[22] Pirzadeh, S., "Structured Background Grids for Generation of Unstructured Grids by Advancing-Front Method", *AIAA Journal*, pp. 257-265, February 1993.

[23] Frink, N. T., Parikh, P., and Pirzadeh, S., "A Fast Upwind Solver for the Euler Equations on Three-

Dimensional Unstructured Meshes", AIAA Paper 91-0102, 1991.

[24] Frink, N. T., Pirzadeh, S., and Parikh, P., "An Unstructured-Grid Software System for Solving Complex Aerodynamic Problems", NASA CP-3291, May 1995.

[25] McCullers, L.A., *FLOPS User's Guide, Release 5.81*, NASA Langley Research Center.

[26] Grasmeyer, J.M., “Stability and Control Derivative Estimation and Engine-Out Analysis”, VPI-AOE-254, Department of Aerospace and Ocean Engineering, Virginia Polytechnic Institute and State University, Blacksburg, Virginia 24061, 1998.

[27] Mattingly, J.D., Heiser, W.H., and Daley, D.H., *Aircraft Engine Design*, AIAA, Washington, D.C., 1987.

[28] Torenbeek, E*., Synthesis of Subsonic Airplane Design*, Delft University Press, Delft, The Netherlands, 1982.

[29] Roskam, J., and Lan, C.-T. E., *Airplane Aerodynamics and Performance*, DARCorporation, Lawrence, KS, 1997.

[30] Vanderplaats, G.N., *Numerical Optimization Techniques for Engineering Design,* Vanderplaats Research & Development, Inc., Colorado Springs, CO, pp.16-22.

[31] Ko, A., “The Role of Constraints and Vehicle Concepts in Transport Design: A Comparison of Cantilever and Strut-Braced Wing Airplane Concepts,” MS Thesis, Virginia Polytechnic Institute & State University, April 2000.